Plasma Sci. Technol. **19** (2017) 115402 (11pp) https://doi.org/10.1088/2058-6272/aa885f

Experimental and simulation investigation of electrical and plasma parameters in a low pressure inductively coupled argon plasma

Jian YANG (杨健)[1], **Angjian WU** (吴昂键)[1], **Xiaodong LI** (李晓东)[1], **Yang LIU** (刘阳)[2], **Fengsen ZHU** (朱凤森)[1], **Zhiliang CHEN** (陈志良)[1], **Jianhua YAN** (严建华)[1], **Ruijuan CHEN** (陈瑞娟)[3] **and Wangjun SHEN** (沈望俊)[3]

[1] State Key Laboratory of Clean Energy Utilization, Institute for Thermal Power Engineering, Zhejiang University, Hangzhou 310027, People's Republic of China
[2] Institute of Physics and Optoelectronics, Dalian University of Technology, Dalian 116024, People's Republic of China
[3] China United Engineering Corporation, Hangzhou 310052, People's Republic of China

E-mail: lixd@zju.edu.cn

Received 13 April 2017, revised 20 August 2017
Accepted for publication 24 August 2017
Published 19 September 2017

Abstract

The electrical and plasma parameters of a low pressure inductively coupled argon plasma are investigated over a wide range of parameters (RF power, flow rate and pressure) by diverse characterizations. The external antenna voltage and current increase with the augment of RF power, whereas decline with the enhancement of gas pressure and flow rate conversely. Compared with gas flow rate and pressure, the power transfer efficiency is significantly improved by RF power, and achieved its maximum value of 0.85 after RF power injected excess 125 W. Optical emission spectroscopy (OES) provides the local mean values of electron excited temperature and electron density in inductively coupled plasma (ICP) post regime, which vary in a range of 0.81 eV to 1.15 eV and 3.7×10^{16} m^{-3} to 8.7×10^{17} m^{-3}, respectively. Numerical results of the average magnitudes of electron temperature and electron density in two-dimensional distribution exhibit similar variation trend with the experimental results under different operating condition by using COMSOL Multiphysics. By comprehensively understanding the characteristics in a low pressure ICP, optimized operating conditions could be anticipated aiming at different academic and industrial applications.

Keywords: ICP, OES, simulation, electrical properties

(Some figures may appear in colour only in the online journal)

1. Introduction

In recent decades, enormous plasma sources based on different electromagnetic mechanisms have been proposed towards diverse industrial applications [1]. Non-thermal plasma sources, including dc glow discharge, gliding arc, dielectric barrier discharge, radio frequency plasma etc [2, 3], emerge as promising techniques with the inherent merits of high chemical selectivity, efficient energy consumption and low gas temperature. Among the most prevailing non-thermal plasma, ICP source, which is initiated and maintained by alternating current, has attracted increasing attention in plasma processing and materials manufacturing due to its benefits of high plasma density, independent adjustment of energy flux, and absence of electrodes interference [4, 5].

Interactions with a time-varying electromagnetic field induced by alternating current induced by radio frequency (RF) power, energy and species conversion are carried out in ICP plasma. The performance of ICP greatly rely on the dissipated energy into plasma exerted by external electrical circuit. Piejak *et al* developed transformer model to analyze ICP electrical properties by considering it as one-turn

secondary of air-core transformer, and indicated the variations of spatial average discharge parameters as function of antenna voltage and current [4]. Hwang *et al* directly calculated the transferred power by comparing the power input at the same current with and without plasma load [6]. Attempts to determine fundamental electrical properties of ICP are achieved in this article over a range of operating condition through monitoring the variation of coil voltage and current. These electrical parameters could be regarded as indexes to estimate the ICP efficiency and plasma electrochemistry activity.

The absorption of power into ICP plasma was conveyed by electrons as most energy is used to generate the free energetic electrons induced by alternating electromagnetic field. Hence the electron density n_e and electron temperature T_e are regarded as two crucial parameters to understand the electron kinetics in plasma, which were assumed to intimately related to the specific reaction rates and products distribution [3, 7]. OES, as a non-intrusive and highly sensitive method, is particularly suitable to gain substantial spectroscopic information in plasma, and to facilitate to provide an insight understanding of the interaction mechanism [8]. Electron temperature T_e is the kinetic temperature of the free electrons, while electron excitation temperature T_{exc} is the electronic excitation temperature of the bound electrons in an atom or a molecule, which governs the distribution of excited states [9]. Electron excitation temperature T_{exc} determined by OES is in good agreement with electron temperature T_e in argon plasmas. The electron temperature is closely related to the electron excitation temperature because of free electrons excitation processes, which govern the distribution of bound electrons excited states in atoms. T_{exc} still could be a good alternative indicator of T_e diagnostics based on their perfect correlation. Khan *et al* comparatively studied the T_{exc} and T_e in E and H modes of ICPs, and indicated similar variation trend of T_{exc} and T_e with applied power and argon pressure [9]. Electron density n_e is calculated by fitting the shape of selected spectral line configuration, which always results in a Voigt profile contributed by convolution of Gaussian broadening (Doppler broadening and instrumental broadening) and Lorentz broadening (Van der Waals broadening and Stark broadening) [10, 11]. By resolving the Lorentz broadening, electron density n_e could be obtained [12].

Simulation model of ICP argon plasma is anticipated necessary to be compared with the experimental measurements, and also provides an alternative to characterize plasma parameters. Recently, self-consistent numerical simulation models derived from in-house code and commercial software are developed to describe the ICP dynamics. Panagopoulos *et al* built a three-dimensional fluid model of ICP and investigated the effect of the azimuthal asymmetries on etch performance [13]. Cheng *et al* used the CFD-ACE+ software to study the sensitivity of structural parameters on the uniformity of plasma parameters based on a regression orthogonal design [14]. Kolovol *et al* discussed possible effects of RF magnetic field on ICP at different driving frequencies with simulation of plasma dynamics, including localized electromagnetic fields at most frequencies [15]. Commercial multiphysics software named COMSOL Multiphysics was employed here, with the consideration of multi-physics process including electromagnetic field and fluid dynamics. The basic package of COMSOL Multiphysics can perform the calculation of fluid dynamics, which treat all species in plasma as continuum to solve complex equations, including species transportation equations, electron energy distribution function and drift diffusion approximation equations, etc. The basic calculation theory is included in [16–18]. Fast and reliable determination of discharged properties could be therefore achieved by tuning various operating conditions in numerical models, reducing the overly burdensome cost from labors and facilities.

In present work, both the experimental and numerical simulation analysis of electrical and plasma parameters in a low pressure ICP are conducted. Influences of different operating conditions (argon pressure, flow rate and RF power) on ICP electrical parameters and power transfer efficiency are investigated in order to provide a comprehensive database to guide the reactor designs towards particular applications. Based on the argon spectrum, T_{exc} and n_e are determined by Boltzmann plot and line-shape fitting, respectively. The effect of operating conditions on the variation of these spectroscopic parameters intrigues our interest, facilitating to promote the understanding of the latent mechanism in specific reactions as well as reaction optimization. The simulation of ICP argon discharged at low pressure is analyzed in terms of spatial distribution of electron temperature, electron density, number density of argon species and flow field based on COMSOL Multiphysics software.

2. Experimental and simulation methods

2.1. Experimental setup

The systematic diagram of ICP argon plasma is depicted in figure 1. The ICP reactor in a cylindrical configuration is constituted of a quartz tube (42 mm in diameter and 750 mm in length), which is surrounded by a 13-turn water-cooled copper antenna. RF power supplied by a 13.56 MHz radio frequency power generator (Kmate, HERO-500W) is delivered to the external antenna through an impedance matching network. The matching box is set in the automatic mode to regulate itself at optimum operating condition of almost zero reflected power. Argon with the purity of 99.9% is selected as carrier gas in the experiments, which is regulated by a mass flow controller (Seven Star D07) in a range of 20–100 sccm. Low pressure in the quartz tube is maintained in a range from 100 mTorr to 1000 mTorr by a rotary pump (KYKY, RVP-2), and was monitored by a vacuum display meter (Inficon AG). The wave forms and magnitudes of antenna voltage and current are measured and recorded by an oscilloscope (Tektronix DPO4034B) with a high-voltage probe (Tektronix P6015A) and a current probe (Tektronix TCP303). An optical spectrometer

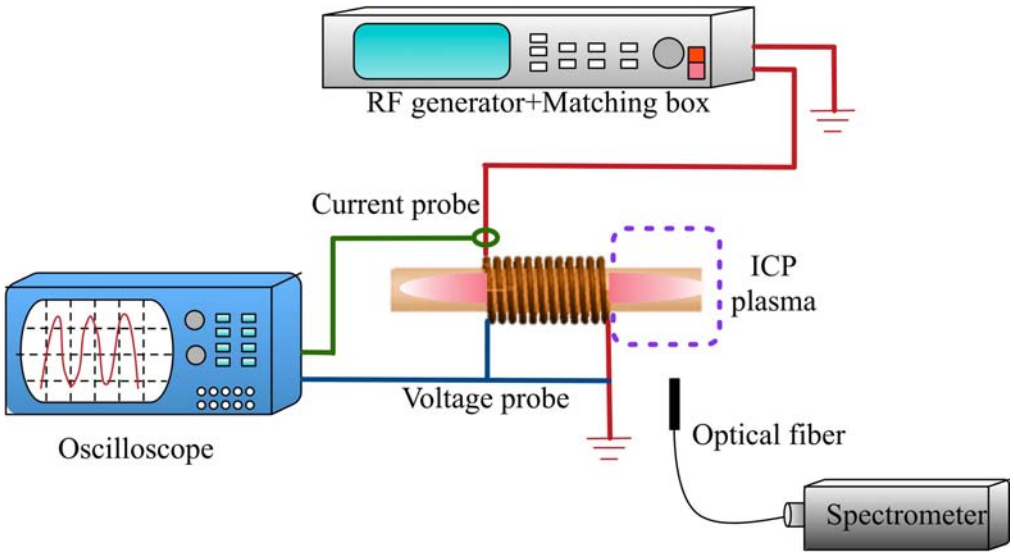

Figure 1. The schematic diagram of ICP argon plasma and diagnostic techniques.

(AvaSpec-ULS) connected with an optical fiber is set in front of ICP plasma, and is used to detect spatial average spectroscopic parameters within the spectral range over 200–1100 nm.

2.2. V-I measurement and electrical parameters calculation

Electrical characteristics of argon ICP at a low pressure is evaluated based on the transformer model by measuring external electric parameters (antenna voltage and current) [19]. With the RF power P_1 delivered into the ICP system, RF voltage with the RMS value V_1 is applied on the antennas, resulting in a primary circuit current I_1 passing through the external helical antenna. The magnitudes of I_1 and V_1 are directly measured by an oscilloscope. According to the transformer model, the external surrounding copper antenna is regarded as the primary winding of the transformer, while the ICP plasma is recognized as the secondary winding of an air-core transformer. The equivalent circuit of the ICP system, which transforms the primary and secondary circuit into a series one in terms of the primary circuit current, is introduced to simplify the theoretical physical process [4]. The power loss P_{Loss} during the transportation process could be expressed as $I_1^2 R_{\mathrm{sys}}$. R_{sys} denotes the effective resistance of system without plasma load, accounting for the total resistance in the matching box, coaxial transmission line and helical antenna [7]. The value of R_{sys} is obtained by applying the RF power on the external circuit without plasma load, expressed as $R_{\mathrm{sys}} = P_0/I_0^2$. The power dissipated in plasma P_{ICP} could be obtained as the difference value between total RF power and loss power, expressed as $P_{\mathrm{ICP}} = P_1 - I_1^2 R_{\mathrm{sys}}$. Hence the plasma resistance R_{P} could be obtained by $R_{\mathrm{P}} = P_1/I_1^2 - R_{\mathrm{sys}}$. In addition, the power transfer efficiency (PTE) η is a significant factor to define the ICP performance, denoted as $\eta = P_{\mathrm{ICP}}/P_1$ [4, 12].

2.3. Spectroscopic diagnostics

Versatile spectroscopic information could be obtained by OES. The intensity of spectral lines I_{nm} describes the transition from upper energy level n to lower energy level m, is regarded as a qualitative indicator of species number density [11, 20].

$$I_{nm} = K_{nm} n_n h \frac{c}{\lambda_{nm}} A_{nm} \tag{1}$$

where K_{nm} is a factor related to plasma volume, λ_{nm} is the wavelength of transition, n_n is the number density at upper level, h is Plank's constant, c is the speed of light, and A_{nm} is emission probability of the transition. The variation of I_{nm} reveals the evolution of the population of related argon species number density through collisional-radiative model with the kinetic reactions as follows [11, 21].

Electron-impact inelastic process, such as ionization and excitation:

$$\mathrm{e} + \mathrm{Ar} \leftrightarrow \mathrm{e} + \mathrm{e} + \mathrm{Ar}^+ \tag{R1}$$

$$\mathrm{e} + \mathrm{Ar} \leftrightarrow \mathrm{e} + \mathrm{Ar}^* \tag{R2}$$

$$\mathrm{e} + \mathrm{Ar}^* \leftrightarrow \mathrm{e} + \mathrm{Ar}^{**} \tag{R3}$$

$$\mathrm{e} + \mathrm{Ar}^* \leftrightarrow \mathrm{e} + \mathrm{e} + \mathrm{Ar}^+. \tag{R4}$$

The heavy particle-impact process:

$$\mathrm{Ar}^* + \mathrm{Ar}^* \leftrightarrow \mathrm{e} + \mathrm{Ar} + \mathrm{Ar}^+. \tag{R5}$$

The radiative de-excitation process:

$$\mathrm{Ar}^+ + \mathrm{e} \rightarrow \mathrm{Ar} + h\nu \tag{R6}$$

$$\mathrm{Ar}^+ + \mathrm{e} \rightarrow \mathrm{Ar}^* + h\nu \tag{R7}$$

$$\mathrm{Ar}^{**} \rightarrow \mathrm{Ar}^* + h\nu \tag{R8}$$

where the rate constants of major reactions of R1, R2, R4 and R5 are $4.0 \times 10^{-12} T_{\mathrm{e}}^{0.5} \mathrm{e}^{-15.8/T_{\mathrm{e}}}$, $1.0 \times 10^{-11} T_{\mathrm{e}}^{0.75} \mathrm{e}^{-11.6/T_{\mathrm{e}}}$, $6.8 \times 10^{-9} T_{\mathrm{e}}^{0.67}$ and 5.0×10^{-10}, respectively [21], and the rate coefficients of R3, R6, R7 and R8 are obtained by solving Boltzmann's equation for the EED [22].

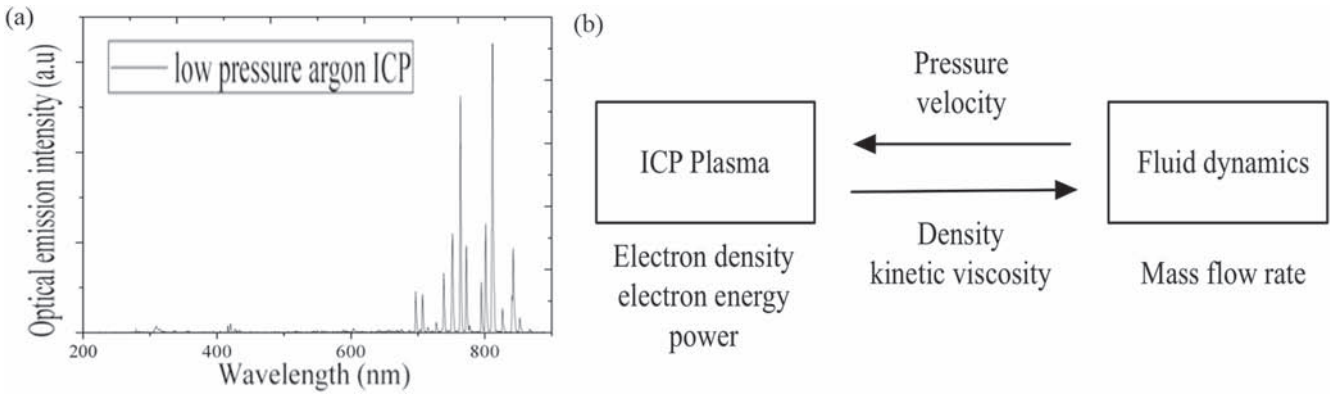

Figure 2. (a) Emission spectra of low pressure argon ICP at power of 50 W and gas pressure of 600 mTorr. (b) The coupling mechanism of multi physics field in low pressure argon ICP process.

Herein Boltzmann distribution of the population of argon atomic levels is assumed [9], providing the relationship between T_{exc} and I_{nm} as follows,

$$\ln\left(\frac{I_{nm}\lambda_{nm}}{g_n A_{nm}}\right) = -\frac{E_n}{kT_{\mathrm{exc}}} + \text{constant} \tag{2}$$

where the g_n is the degeneracy of upper state n, E_n is the excitation energy of upper state, and k is the Boltzmann constant. Taking the $\ln\left(\frac{I_{nm}\lambda_{nm}}{g_n A_{nm}}\right)$ as the ordinate and E_n as the abscissa, T_{exc} could be obtained by calculating the slope rating using a Boltzmann plot.

The full argon spectra dominated by atomic argon lines due to 4s–4p ranging from 200 nm to 900 nm is illustrated in figure 2(a) [23]. Amongst, the configuration of the spectral argon line at 696.5 nm depends on plasma temperature and electron density is analyzed by fitting in a Voigt profile. The Voigt profile is contributed to the convolution of Lorenz broadening (w_{L}) and Gaussian broadening (w_{G}) as follows:

$$w_{\mathrm{G}}^2 = w_{\mathrm{D}}^2 + w_{\mathrm{in}}^2 \tag{3}$$

$$w_{\mathrm{L}} = w_{\mathrm{S}} + w_{\mathrm{v}} \tag{4}$$

where w_{G} is contributed by Doppler broadening (w_{D}) and instrumental broadening (w_{in}), and w_{L} is constituted by Stark broadening (w_{S}) and Van del Waals broadening (w_{v}). The plasma temperature and electron could be obtained through formulas (5) and (6), whereas the detailed mechanism and calculation method in [11, 23, 24] will not be elaborated here:

$$w_{\mathrm{D}} = 7.16 \times 10^{-7}\lambda\left(\frac{T_{\mathrm{P}}}{M}\right)^{1/2} \tag{5}$$

$$w_{\mathrm{S}} = 2 \times [1 + 1.75 \times 10^{-4} N_{\mathrm{e}}^{1/4}\alpha \times (1 - 0.068 N_{\mathrm{e}}^{1/6} T_{\mathrm{e}}^{-\frac{1}{2}})] 10^{-16} w_{\mathrm{e}} N_{\mathrm{e}} \tag{6}$$

where M is the mass of the radiating atom, α is the parameter that characterized the quasi-static ion broadening, w_{e} is the half width at half maximum (HWHM) [25].

2.4. Numerical theory and boundary conditions

A 2D axisymmetric model of ICP reactor is calculated into three parts consisting of plasma, coil group and surrounding regime, with separate meshes constituted. Notably, the EEDF deviates from the Maxwellian in a low pressure ICP with some rate coefficients in sensitive dependence on deviations from the Maxwellian equations. Hence the Boltzmann equation is selected to calculate different local values, which is more appropriate at a low pressure condition [26]. Because the electron distribution function is almost isotropic in velocity field, which is determined by local values of the electric field, electron density, and plasma composition [27]. In continuum equations of fluid dynamics, related electron transport coefficients and reaction rates can be obtained by the local Boltzmann solver in COMSOL Multiphysics [28]. With the consideration of gas heating effects, velocity slips and temperature jumps could occur at walls [29]. The wall adjacent to the plasma is set zero potential (ground connection), while the external boundaries of modeled regime is set magnetically insulated [30]. Hence argon chemistry is considered, which is related to collisions between electrons, ions, excited atoms and neutral atoms. The gas flow rate and pressure are set according to experiment designs. The complex equations consist of species transportation equations, electron energy distribution function and drift diffusion approximation equations etc., which govern ICP plasma physics and fluid flows solving based on fluid model and summarized as follows:

Drift diffusion equations are used to calculate the transportation of electrons and electrons energy [17, 18]:

$$\frac{\partial(n_{\mathrm{e}})}{\partial t} + \nabla \cdot \boldsymbol{\Gamma}_{\mathbf{e}} = R_{\mathrm{e}} - (\boldsymbol{u} \cdot \nabla) n_{\mathrm{e}} \tag{7}$$

$$\frac{\partial(n_{\varepsilon})}{\partial t} + \nabla \cdot \boldsymbol{\Gamma}_{\varepsilon} + \boldsymbol{E} \cdot \boldsymbol{\Gamma}_{\mathbf{e}} = R_{\varepsilon} - (\boldsymbol{u} \cdot \nabla) n_{\varepsilon} \tag{8}$$

where the n_{e} and n_{ε} are the electron density (m^{-3}) and electron energy density ($\mathrm{eV/m}^3$), respectively. $\boldsymbol{\Gamma}_{\mathbf{e}}$ and $\boldsymbol{\Gamma}_{\varepsilon}$ are the flux of electrons and electron energy due to the electric field and diffusion. Due to the collisions and reactions occurred in plasma, R_{e} and R_{ε} are separately introduced as the generation rate of electrons and the gain (or loss) of the energy. While the $(\boldsymbol{u} \cdot \nabla) n_{\mathrm{e}}$ and $(\boldsymbol{u} \cdot \nabla) n_{\varepsilon}$ are the convective term, and $\boldsymbol{u}$ is the velocity of neutral fluid. The flux terms ($\boldsymbol{\Gamma}_{\mathbf{e}}$ and $\boldsymbol{\Gamma}_{\varepsilon}$) depended on ambipolar diffusion and electrical field migration are as follows:

$$\mathbf{\Gamma_m} = -n_m(u_m \cdot \boldsymbol{E}) - D_m \cdot \nabla n_m \tag{9}$$

where the n_m represents the density, u_m represents the mobility, D_m represents the diffusivity. m = e and ε refer to electron and electron energy, respectively.

The heavy species, which consisted of neutrals, ions and excited state of argon, are considered as follows:

$$\rho\frac{\partial(w_k)}{\partial t} + \rho(\boldsymbol{u} \cdot \nabla)w_k = \nabla \cdot \boldsymbol{j_k} + R_k \tag{10}$$

where w_k and $\boldsymbol{j_k}$ are the mass fraction and diffusive flux of species k, respectively. $\boldsymbol{u}$ is the mass averaged fluid velocity vector, ρ is the density of the mixture, and R_k is the generation rate coefficient for the species k. Similar to the calculation, a mixture-averaged model is applied to solve equation (10) [17, 30]. Detailed descriptions of heavy species transportation could be found in user's guide of COMSOL Multiphysics [16]. It is worth noting that wall reaction from quench of heavy species (metastable argon atoms Ars and argon ion Ar^+) is very important and regarded as Ars = >Ar and Ar^+ = >Ar in software (Ars include Ar^* and Ar^{**}).

The electrostatic field is solved according to Possion's equation:

$$-\nabla \cdot \varepsilon_0\varepsilon_r\nabla V = \rho \tag{11}$$

where ε_0 and ε_r are the vacuum permittivity and relative permittivity, respectively, and V represents the electrical potential. The space charge density $\rho = q(\sum_{k=1}^{N} Z_k n_k - n_e)$ is based on the ICP argon plasma chemistry. Where q means the elementary charge, n_k means the density of ions, and Z_k is the charge number. Ampere's law is employed to solve the electromagnetic field in ICP [30]:

$$(\mathrm{j}\omega\sigma - \omega^2\varepsilon_0\varepsilon_r)\boldsymbol{A} + \nabla \times (\mu_0^{-1}\mu_r^{-1}\nabla \times \boldsymbol{A}) = \boldsymbol{J}_e \tag{12}$$

where the j and ω are the imaginary unit and angular frequency of the electric source, respectively. σ is the electric conductivity, and $\boldsymbol{A}$ and $\boldsymbol{J_e}$ are the magnetic vector and applied external current, respectively. Hence, the induced electric filed could be described as $\boldsymbol{E} = -\mathrm{j}\omega\boldsymbol{A}$.

Due to low pressure and total flow rate considered in system, Laminar flow is applied to describe the argon flow through the ICP plasma regime, by considering continuity equation and momentum equation.

$$\frac{\partial\rho_m}{\partial t} + \nabla \cdot (\rho_m \boldsymbol{u}_\mathbf{v}) = 0 \tag{13}$$

$$\rho_m\frac{\partial \boldsymbol{u}_\mathbf{v}}{\partial t} + \rho_m(\boldsymbol{u}_\mathbf{v} \cdot \nabla)\boldsymbol{u}_\mathbf{v} = \nabla \cdot [-p\boldsymbol{L} + \mu_\mathrm{D}\left(\nabla\boldsymbol{u}_\mathbf{v} + (\nabla\boldsymbol{u}_\mathbf{v})^T - \tfrac{2}{3}\mu_\mathrm{D}(\nabla\boldsymbol{u}_\mathbf{v})\boldsymbol{L}\right] + \boldsymbol{F} \tag{14}$$

where the ρ_m presents the density, the $\boldsymbol{u}_\mathbf{v}$ presents the velocity, and the μ_D is the viscosity, while the $\boldsymbol{F}$ and $\boldsymbol{L}$ are the force vector and identity matrix, respectively. And the no-slip wall is set as the boundary condition. p was the pressure at the outlet, which was set according to the vacuum used.

3. Results and discussions

3.1. V-I characteristics and electrical parameters

Figure 3(a) indicates the similar trend of antenna coil and current depending on RF power. The measured antenna current gains one-fold increase with the enhancement of RF power from 50 W to 300 W. The antenna voltage initially drops from about 372.5 V to 355.5 V with the RF power injected from 50 W to 75 W, and then almost increases monotonically from 348 V to 535 V with the increase of RF power. The increase of RF power results in the enhancement of RF magnetic flux, which in return requires an increase of antenna current. In addition, aforementioned positive *V-I* behavior might be due to the antenna leakage inductance [1], which is a common phenomenon in low pressure ICP plasma due to a loose antenna coupling to plasma [19]. And relative strong effect of leakage inductance here counteracts the negative *V-I* effect caused by plasma negative differential impedance. Obviously, the variation of plasma resistance is non-monotonous with the linear increase of plasma adsorbed energy, which can be accounted for the competition of two factors, an increase in the electron number participating in power absorption with increasing electron density and a decrease in this number due to a decrease in skin depth leading uniform electromagnetic field [31]. In figure 3(b), it is demonstrated that the power transfer efficiency increases obviously from 0.6 to 0.85 with the total RF power increasing from 50 W to 125 W. Poor power conversion is obtained with 50 W power input, implying almost 40% of energy is dissipated in heating of system resistance rather than increasing the electron energy and density, or initiation of plasma reactions. On the other hand, the power transfer efficiency tends saturation at 0.85 since the RF power exceeds 125 W, which indicates a better performance of ICP power conversion is achieved at relatively high power. When the current passing through coils increases due to the increase of RF power, the plasma absorbed power increases by a factor of 8, whereas the power consumed in system varies only by a factor of 2.5, indicating the coupling between external antenna coil and plasma improved with the increase of RF power.

The influence of gas pressure on the electrical parameters is illustrated in figure 4. Both antenna coil current and voltage decline with the increase of gas pressure, which is similar to the trend observed in [1, 4]. For a given RF power and gas flow rate, relatively larger current and voltage are required at lower gas pressure to sustain the plasma, which resulted in more fraction of energy dissipated in the system such as ohmic heating of antenna, leading to lower power transfer efficiency obtained. On the other hand, increasing the gas pressure improves the performance of power conversion in accompany with the increase of the plasma resistance. It is because that the collision frequency between electrons and neutrals are relatively weak at low pressure, which resulted in a low plasma conductivity and a relatively low plasma absorbed power [32]. Hence, increasing pressure appropriately facilitated the power conversion by promoting the electron generation, but its effect was somewhat less efficient compared to that of adjustment of RF power.

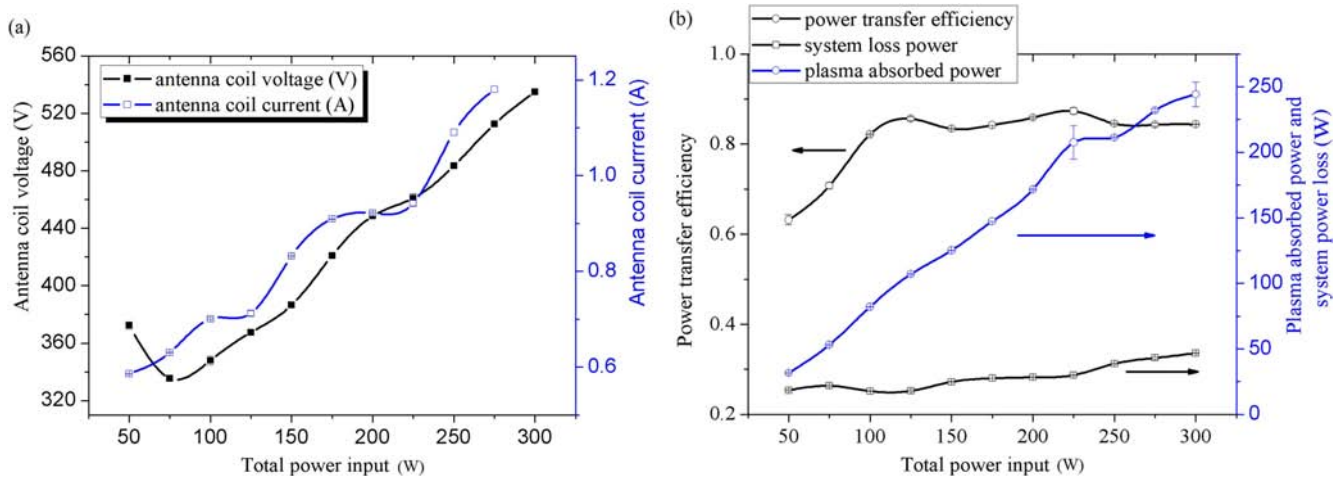

Figure 3. (a) Antenna coil current and voltage versus total RF power. (b) The power transfer efficiency, plasma absorbed power and system loss power as a function of total RF power injected (gas flow rate = 20 sccm, pressure = 100 mTorr).

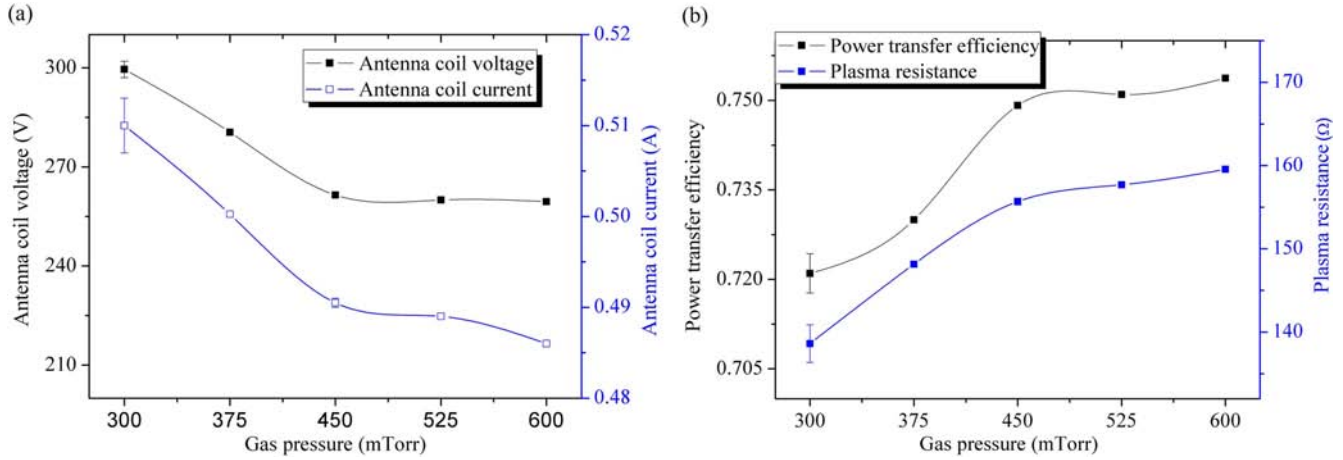

Figure 4. (a) Antenna coil current and voltage versus gas pressure. (b) The power transfer efficiency and plasma resistance as a function of gas pressure (gas flow rate = 20 sccm, RF power = 50 W).

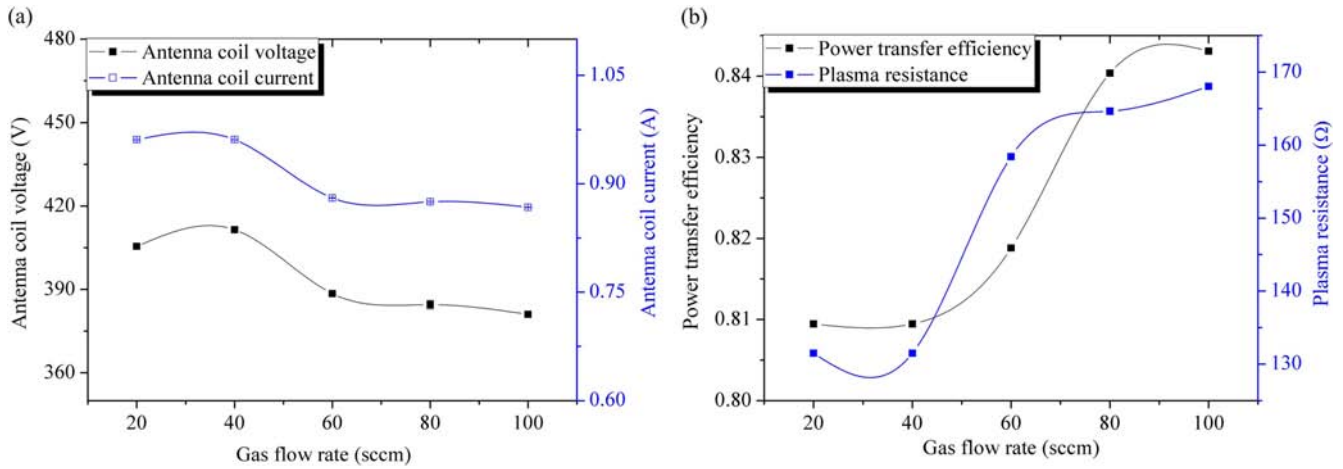

Figure 5. (a) Antenna coil current and voltage versus gas flow rate. (b) The power transfer efficiency and plasma resistance as a function of gas flow rate (gas pressure = 600 mTorr, RF power = 150 W).

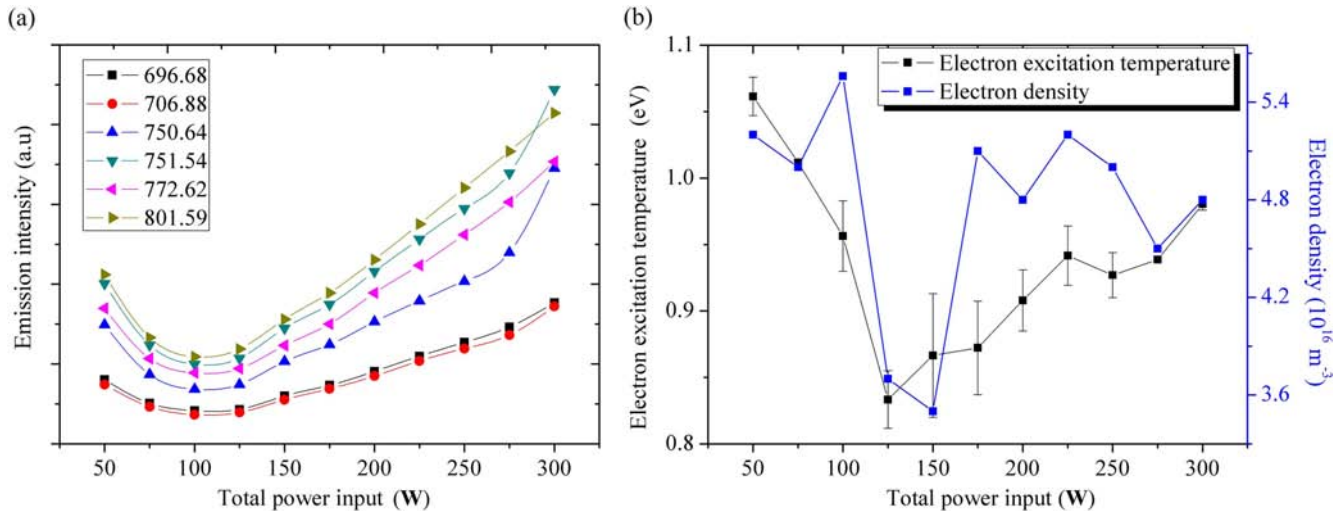

Figure 6. (a) The dependence of emission line intensity on the total power input. (b) The dependence of electron excitation temperature and electron density on the total power input (gas pressure = 100 mTorr, gas flow rate = 20 sccm).

When the gas pressure and RF power are set at 600 mTorr and 150 W, respectively, the relevance of electrical parameters with gas flow rate is indicated in figure 5(a). And this operating condition is also suitable for the growth of graphene from methane in our recent research work [33]. The variation trends of antenna coil voltage and current are synchronous almost at any gas flow rate. With the augment of gas flow rate, both the voltage and current increase at first and then decline, and reach the maximum value at gas flow rate of 40 sccm. And the variation amplitudes of 9% are not notable. With the augment of gas flow rate from 20 sccm and 100 sccm in figure 5(b), power transfer efficiency and the plasma resistance increase from 0.81 to 0.84 and from 130 Ω to 168 Ω, respectively. As argon flow rate increases, number density turns to grow up, which might promote the collision frequency between electrons and argon atoms, resulting in the enhancement of energy transfer from electric field to internal plasma energy. In addition, penning effect could be improved to facilitate the generation of energetic electrons and argon metastable atoms, which somewhat helps to increase plasma resistance and plasma density.

3.2. Optical emission characteristics, electron excitation temperature and electron density obtained by OES

OES, as a non-intrusive and highly sensitive method, is particularly suitable to gain substantial spectral information and to provide an insight understanding of the interaction mechanism under different operating circumstances. The optical emission spectrum ranging from 178 nm to 890 nm is obtained by an optical fiber, which is positioned perpendicular to the post ICP coil regime with a distance of 5 cm indicated in figure 1.

The dependence of spectroscopic parameters on the RF power, gas pressure and gas flow rate are investigated based on the emission intensity and line profile. According to figure 6(a), the emission intensity of six argon atomic lines from the 4s–4p transition presents as a function of RF power. When the RF power is below 100 W, sorts of 'faint glow' plasma is observed between the copper coil regimes. And abnormal phenomenon is detected that the emission intensity decreases with power injected. With the enhancement of RF power from 100 W to 300 W, the emission intensity of all these spectral lines increases linearly, exhibiting contrary trend to that at low RF power condition as more excitation transition radiation takes place [20]. And luminous pink glow plasma is observed through the entire quartz tube. Thus, it indicates the power input affects the population density of argon excited state significantly, as the emission intensity is regarded as an indicator of species number density at certain metastable state. In figure 6(b), both the electron excitation temperature (T_{exc}) and electron density (n_e) present similar trend to the variation of RF power. The negative dependence of T_{exc} and n_e on power injected is observed below 125 W in accordance with emission intensity, as a consequence of increasing effect of step-wise ionization and electron-electron collisions. However, with further increasing power from 125 W to 300 W, more energy is absorbed by plasma and transferred into electrons and argon by strengthening the elastic and inelastic electron-neutral collisions, bringing up the mean T_{exc} and n_e from 0.83 eV to 0.98 eV and from 3.7×10^{16} m^{-3} to 5.2×10^{16} m^{-3}, respectively.

The influence of gas flow rate on emission intensity is presented in figure 7(a), which shows that the emission intensity of argon lines increases accompanied with the enhancement of gas flow rate. The spectral lines at different wavelength present similar variation trend, whereas the magnitudes of emission intensity at different wavelength are different due to different cross-section for excitation, amongst the light intensity at wavelength of 801.6 nm is strongest. On one hand, higher argon flow rate raises the number density of argon, resulting in an increase of collision probability and intensified penning effect by indirect excitation or two-step excitation process, facilitating the energy to transfer from electromagnetic field into plasma [34]. On the other hand, higher flow rate causes stronger cooling effect, accelerating the electron de-excitation and weakening the

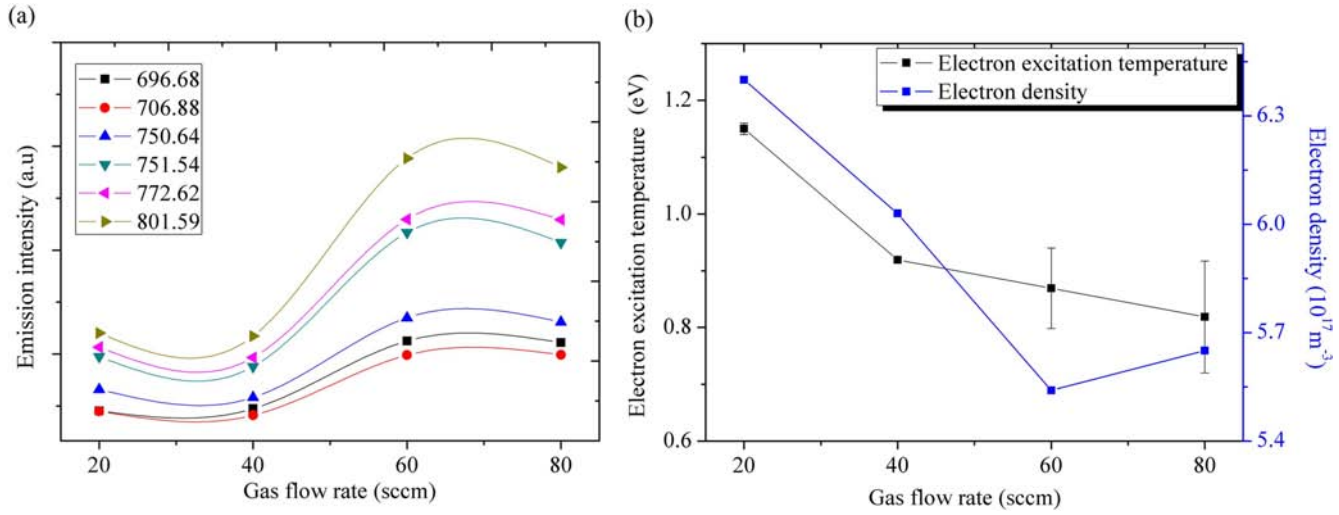

Figure 7. (a) The dependence of emission line intensity on the gas flow rate. (b) The dependence of electron excitation temperature and electron density on gas flow rate (total input power = 50 W, gas pressure = 600 mTorr).

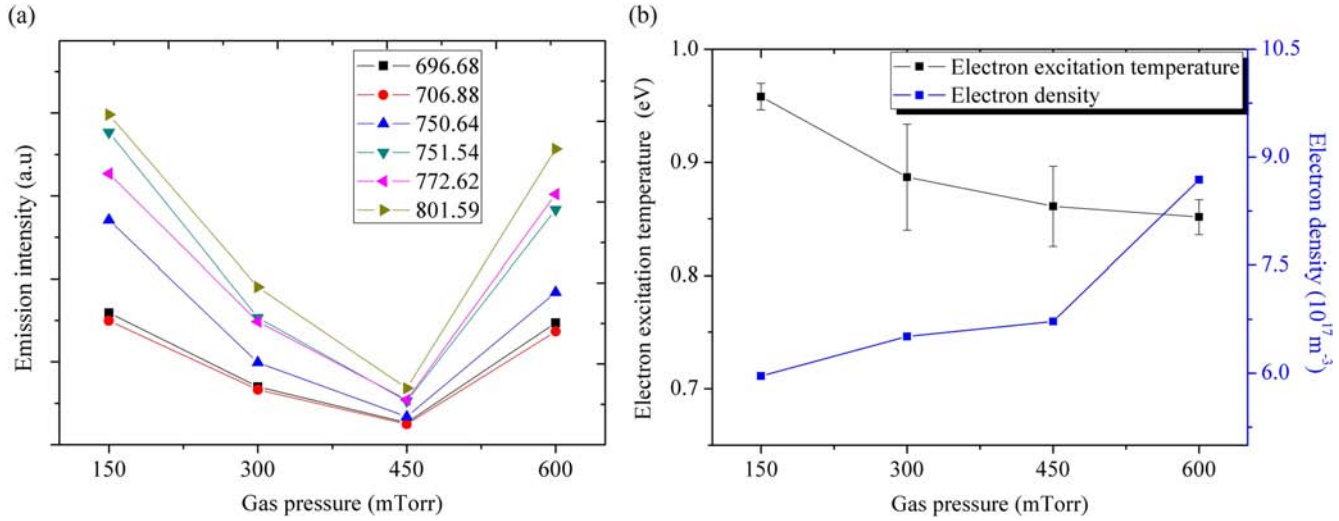

Figure 8. (a) The dependence of emission line intensity on the gas pressure. (b) The dependence of electron excitation temperature and electron density on gas pressure (total input power = 250 W, gas flow rate = 20 sccm).

excitation by direct electron collisions, therefore the decreasing tendency of emission intensity occurs at gas flow rate of 80 sccm. With the gas flow rate increasing from 20 sccm to 80 sccm in figure 7(b), mean T_{exc} reduces almost 30% from 1.15 eV to 0.81 eV, while n_e decreases from 6.4×10^{17} m^{-3} to 5.65×10^{17} m^{-3}. That is to say, augment of gas flow rate in ICP would decline the density of high excited electrons and shift shape of electron energy distribution function to low mean energy level in terms of T_{exc}. And the negative effect of gas flow rate on n_e is induced by interactions of increasing gas with neutral argon atoms and enhanced cooling effect as well.

The dependence of emission intensity on the gas pressure is demonstrated in figure 8(a). With the gas pressure increases from 150 mTorr to 450 mTorr, the emission intensity decreases at first, and then increases with further augment of gas pressure from 450 mTorr to 600 mTorr, which is determined and balanced by electron energy and collision frequency in ICP. As shown in figure 8(b), varying gas pressure exerts two opposite effects on T_{exc} and n_e. Increasing the gas pressure from 150 mTorr to 600 mTorr, T_{exc} decreases from 0.96 eV to 0.85 eV, whereas the n_e increases from 5.9×10^{17} m^{-3} to 8.7×10^{17} m^{-3}. Such behavior is common for gas discharge as higher gas pressure means higher species density in unit volume, which reduces the average mean free path of electron [9]. The mean kinetic energy of electrons is reduced by insufficient acceleration of electric field and energy loss due to collisions, resulting in the falling pressure dependence of T_{exc}. Concurrently, with the increasing of gas pressure, plasma density and n_e increase significantly with the increase of power transfer efficiency.

3.3. Simulation results

The operating conditions designed in simulations are consistent with experiments. Two-dimensional distributions of velocity field, electron temperature, electron density, number density of excited argon atoms and number density of neutral

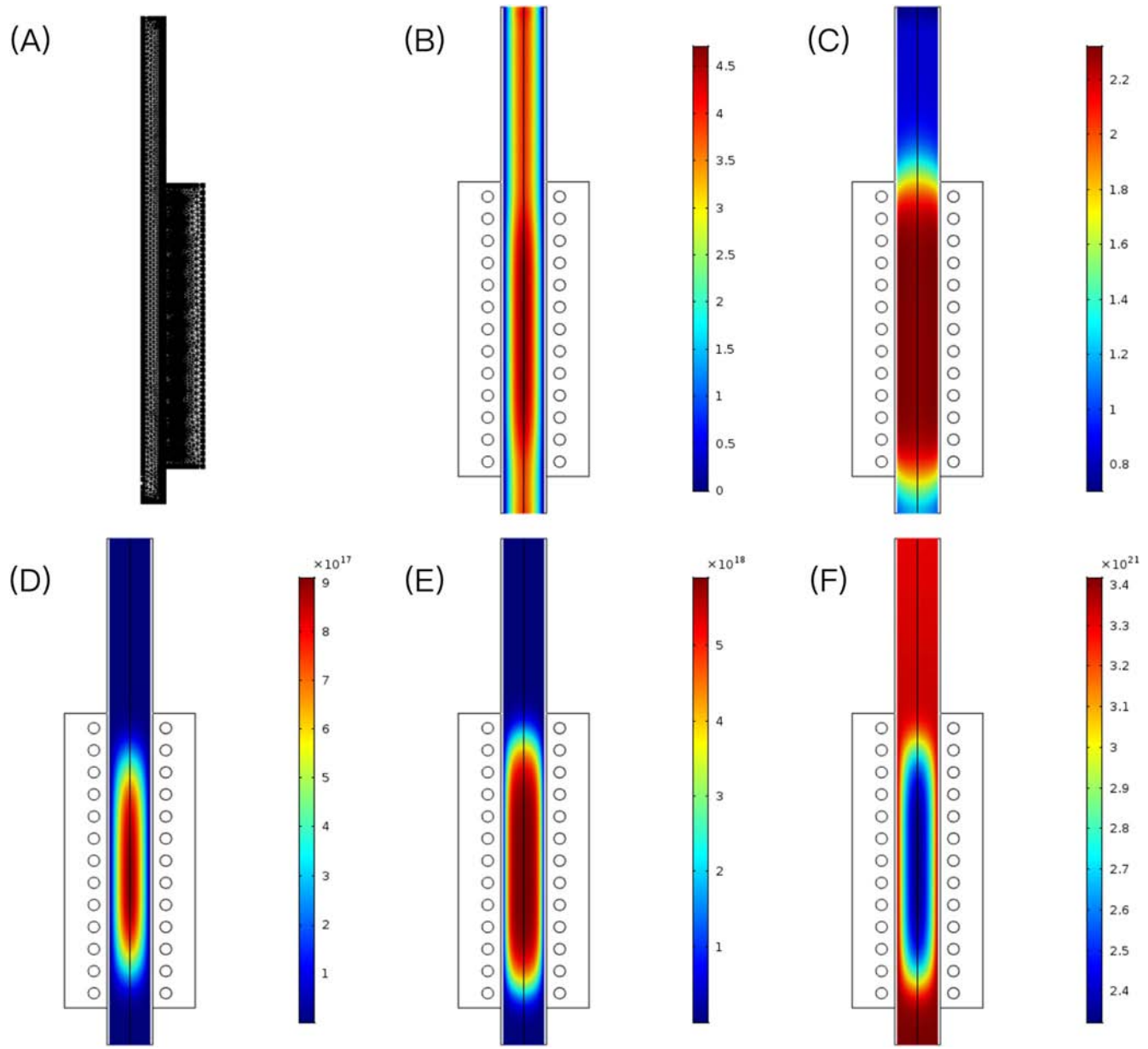

Figure 9. (A) Mesh built for ICP reactor, (B) velocity field distribution ($m \cdot s^{-1}$), (C) electron temperature distribution (eV), (D) electron density distribution (m^{-3}), (E) number density of excited argon atoms distribution (m^{-3}), (F) number density of neutral argon atoms distribution (m^{-3}) (gas pressure = 600 mTorr, gas flow rate = 20 sccm, RF power = 150 W).

argon atoms are demonstrated in figure 9. The magnitudes of electron density, temperature and argon number density are the volume average values in figure 10. The convergence is achieved on Intel Core i7 with 4 CPU for 1 h. The gas flow rate and pressure are set at 20 sccm and 600 mTorr, respectively. The initial temperature and RF power input are set at 300 K and 250 W, respectively.

In figure 9, the laminar flow distribution is depicted in (B), and the maximum velocity is achieved inside the quartz tube between the third and the eighth RF coil turning along the axial direction, which is attributed to concentrating electromagnetic heating inside [35]. The profile of electron temperature is in a quasi-uniform distribution with the most intense region above 1.8 eV. Meanwhile, the electron density also follows the profile of electron temperature, forming a narrow and ellipsoidal distribution, implying the most intense coupling effect between coil and plasma. A great steep gradient of electron density along radial direction is observed due to the effect of plasma sheath near the wall. Based on the high electron temperature and electron density, the majority of excited argon atoms are prone to be generated in the dense electron region, therefore, resulting into a similar distribution profile of number density of excited argon atoms with electron density. The largest number density of neutral argon atoms appears at inlet, and then fast decreases due to excitation and ionization via R1 and R2. Hence, the distribution of neutral argon is approximately in contrast to that of excited argon atoms.

For materials fabrication by ICP such as graphene, nanotube and hybrid carbon material, pressure and power are the most crucial factors to tune the morphology and structure

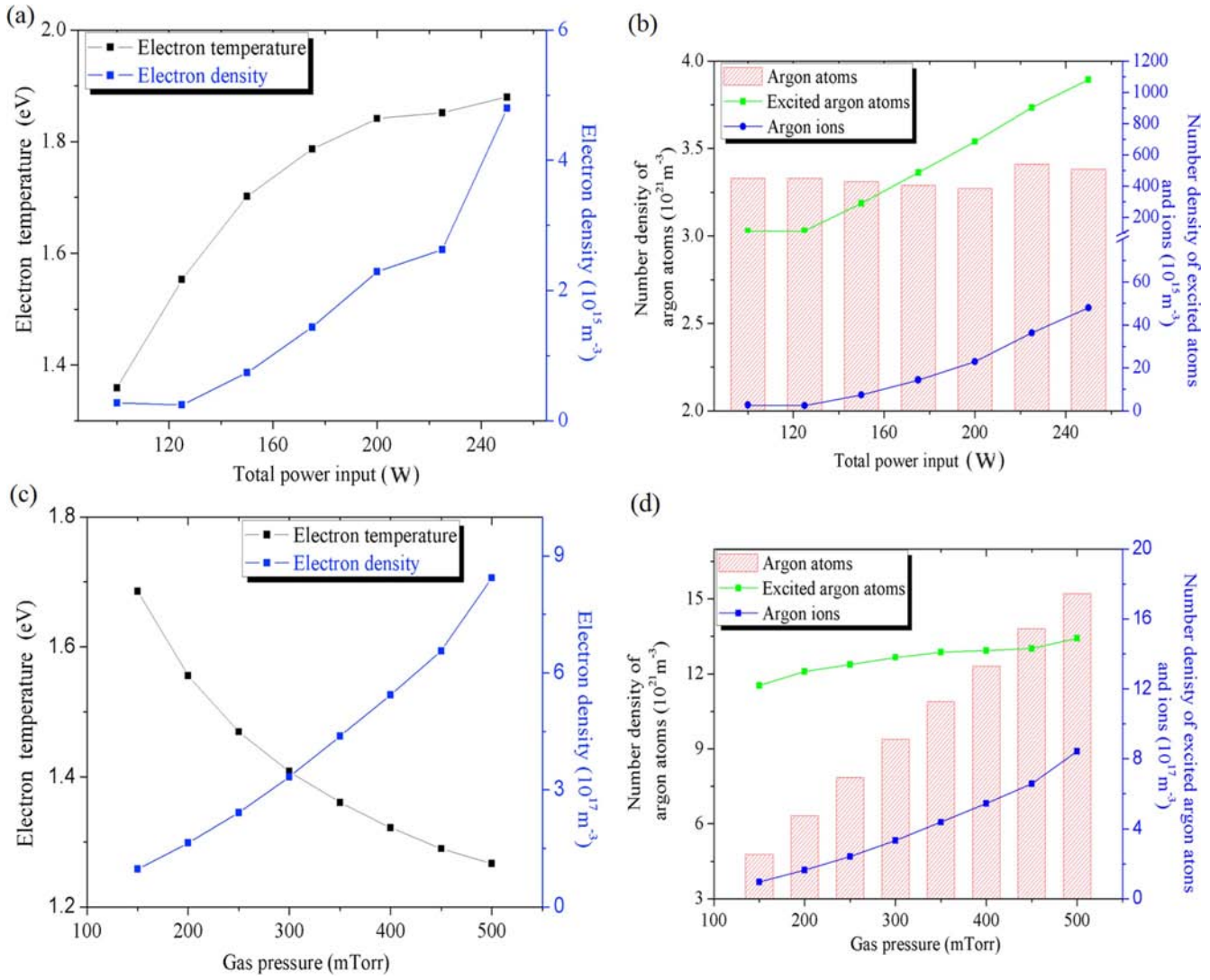

Figure 10. The influence of RF power ((a), (b)) and gas pressure ((c), (d)) on the electron temperature, electron density and the number densities of argon atoms, excited argon atoms and argon ions (volume-averaged).

of products for different applications. Hence, the influences of power and pressure on different plasma parameters are calculated by simulation. According to the calculation indicated in figure 10, the effects of power input and gas pressure on the electron temperature and density are notable. Increasing total power input under fixed gas pressure and flow rate of 100 mTorr and 20 sccm, respectively, the electron density and temperature rose from 2.7×10^{15} m^{-3} to 4.8×10^{18} m^{-3} and from 1.3 eV to 1.8 eV, respectively, which exhibits good agreement with the variation trend in experiment results. At higher electron energy and more frequent electron collisions, the number density of excited argon atoms increases by R2 due to the low threshold of 11.5 eV for excitation. The augment of density of argon ions is deduced mainly by R1 and R4 as well as penning effect in R5. The density of total neutral argon atoms is generally unchanged and balanced by the ionization, excitation and de-excitation process. With the pressure increasing from 150 mTorr to 600 mTorr under the power and flow rate of 250 W and 20 sccm, respectively, the electron temperature reduces approximately 25% from 1.6 eV to 1.2 eV, while the electron density increases nearly 5-fold magnitude, which indicates the pressure gas pressure plays a determinant role in the variation of electron density and temperature. Meanwhile, accompanied with the greatly increase of argon atoms number per volume, excited argon atoms are inclined to transfer the stored energy into ions or gas temperature by R4 and R5, leading to the decrease of number density of argon excited atoms and the increase of number density of argon ions simultaneously.

4. Conclusions

The low pressure argon ICP plasma is comprehensively investigated by both the experiments and simulation. Electrical parameters (plasma resistance, plasma absorbed power and power transfer efficiency) are estimated by measuring external antenna coil voltage and current. And the numbers of electron density and electron excitation temperature can be calculated according to argon line profile and Ar I intensity.

Energy transfer efficiency is promoted at low RF power, and then becomes saturated at about 0.85 eV with further increasing power. However, the mean T_{exc} and n_e continues to increase from 0.83 eV to 0.98 eV and from 3.7×10^{16} m^{-3} to 5.2×10^{16} m^{-3}, respectively. Plasma resistance enhances from 130 Ω to 168 Ω by intensified collisions effect induced by augment of gas flow rate, whereas decrease of T_{exc} and n_e from 1.15 eV to 0.81 eV and from 6.4×10^{17} m^{-3} to 5.65×10^{17} m^{-3} by intensified cooling effect due to gas flow. Increasing gas pressure prominently lifts n_e by greatly improving the collision frequency, while reduces the T_{exc} due to reducing electron free path in contrast. Two-dimensional distribution of plasma parameters are depicted based on COMSOL Multiphysics, and similar variation tendency of calculation results are obtained compared to OES observation. When the RF power increases from 100 W to 250 W, the electron temperature increases 38% and gradually turns saturated beyond 200 W, while the number density of all species increases greatly except for the neutral argon atoms. When the gas pressure increases from the 100 mTorr to 500 mTorr, the electron density shows an abruptly increase of one magnitude, whereas the electron temperature declines from 1.6 eV to 1.2 eV in contrast.

Acknowledgments

This work is supported by National Natural Science Foundation of China (No. 51576174).

References

[1] Godyak V A 2011 *Plasma Sources Sci. Technol.* **20** 1959
[2] Fridman A, Chirokov A and Gutsol A 2005 *J. Phys. D: Appl. Phys.* **38** 1
[3] Wu A J *et al* 2014 *Int. J. Hydrogen Energy* **29** 17656
[4] Piejak R B, Godyak V A and Alxandrovich B M 1992 *Plasma Sources Sci. Technol.* **1** 179
[5] Godyak V A, Piejak R B and Alexandrovich B M 2002 *Plasma Sources Sci. Technol.* **11** 525
[6] Hwang H J, Kim Y C and Chung C W 2013 *Thin Solid Films* **547** 9
[7] Park S *et al* 2015 *Plasma Sources Sci. Technol.* **24** 034003
[8] Wu A J *et al* 2014 *IEEE Trans. Plasma Sci.* **42** 2560
[9] Khan A W *et al* 2013 *Curr. Appl. Phys.* **13** 1241
[10] Christova M, Gagov V and Koleva I 2000 *Spectrochim. Acta.* B **55** 815
[11] Wu A J *et al* 2015 *IEEE Trans. Plasma Sci.* **43** 836
[12] Park S *et al* 2014 *Appl. Phys. Lett.* **104** 084103
[13] Panagopoulos T *et al* 2002 *J. Appl. Phys.* **91** 5
[14] Cheng J, Zhu Y and Ji L H 2012 *Plasma Sci. Technol.* **14** 1059
[15] Kolobov V I and Godyak V A 2017 *Plasma Sources Sci. Technol.* **26** 075013
[16] Plasma Module User's Guide version 5.2 COMSOL Inc. (www.comsol.com)
[17] Brezmes A O and Breitkopf C 2014 *Vacuum* **109** 52
[18] Tong L Z and Nanbu K 2006 *Europhys. Lett.* **75** 63
[19] Godyak V A, Piejak R B and Alexandrovich B M 1999 *J. Appl. Phys.* **85** 703
[20] Czerwiec T and Graves D B 2004 *J. Phys. D: Appl. Phys.* **37** 2827
[21] Moravej M *et al* 2006 *Plasma Sources Sci. Technol.* **15** 204
[22] Bhoj A N and Kushner M J 2004 *J. Phys. D: Appl. Phys.* **37** 2510
[23] Iordanova S and Koleva I 2007 *Sectrochim. Acta.* B **62** 344
[24] Pellerin S *et al* 1996 *J. Phys. B: At. Mol. Opt. Phys.* **29** 3911
[25] Hopwood J 1994 *Plasma Sources Sci. Technol.* **3** 460
[26] Mouchtouris S and Kokkoris G 2016 *Plasma Sources Sci. Technol.* **25** 025007
[27] Kolobov V I and Arslanbekov R R 2006 *IEEE Trans. Plasma Sci.* **34** 895
[28] Hagelaar G J M and Pitchford L C 2005 *Plasma Sources Sci. Technol.* **14** 722
[29] Arslanbekov R, Kolobov V and Zhou N 2003 Kinetic simulations of capacitively coupled plasmas with external circuit *56th Gaseous Electronics Conf.* (American Physical Society) p 158
[30] Brezmes A O and Breitkopf C 2015 *Vacuum* **116** 65
[31] Kralkina E A *et al* 2016 *Plasma Sources Sci. Technol.* **25** 015016
[32] Griem H R 1964 *Plasma Spectroscopy* (New York: McGraw-Hill)
[33] Angjian W *et al* 2017 *Appl. Energy* **195** 67
[34] Stewart R S and Smith D J 2002 *J. Phys. D: Appl. Phys.* **35** 1777
[35] Hanene B *et al* 2014 *Phys. Scr.* **T161** 014008